This month in GEOPHYSICS

J.P. Lindsey, Editor

Electromagnetics

Boerner et al. discuss the interpretation of controlled source EM data in terms of the orthogonality of the electric and magnetic fields. They show that nonorthogonality is a sensitive indicator of geologic structure and demonstrate a quantitative analysis of the galvanic scattering response caused by surficial features.

Gravity

Guspí derives an exact inverse series from Parker's forward expression for the rapid calculation of potential anomalies, thereby enabling simultaneous gravity inversions with a variety of density contrasts.

Borehole geophysics

Bjarnason and Menke use the method of projection onto convex sets (POCS) to provide a flexible and numerically efficient means of imposing prior constraints in tomographic imaging. When applied to cross-borehole tomography, images with fewer artifacts (such as streaks) than other methods can be achieved.

Seismic theory

Kosik uses an implicit 2-D finite-difference algorithm to simulate the nonlinear propagation of a cylindrically symmetric pulse through an anelastic medium. He finds that the nonlinear anelastic pulse near the source has an amplitude that is several times larger and a propagation velocity that is slightly less than a linear pulse. In an experiment on a simulated (parallel) fractured medium, **Hsu and Schoenberg** measure ultrasonic elastic wave velocities in several directions. The five elastic moduli of the long wavelength equivalent transversely isotropic medium, obtained from the velocities, fit the predictions of the linear slip deformation model, allowing these moduli to be expressed in terms of two pressure-independent isotropic background elastic moduli and two pressure-dependent slip parameters related to fracture response.

Seismic modeling

When seismic wave propagation in anelastic earth layers with transverse isotropy is modeled, the geophysicist often has incomplete knowledge of the material constants that describe the formations to be encountered in the subsurface. To avoid physically unrealizable materials and the computational artifacts that they can generate, **Rosenbaum** suggests stability criteria and empirically reasonable default parameter values to be applied at the input of a modeling program. **Fischer and Lees** suggest several improvements to the shortest path ray-tracing technique to increase the efficiency of graph-based methods. These include implementing Snell's Law at interfaces, an algorithm that avoids undetermined solutions and a quantitative assessment of the minimum number of nodes required for accurate ray tracing.

Seismic data processing

Reiter et al. describe a method for inverting and imaging two-dimensional velocity functions. The technique requires the recording of post-critically reflected and refracted arrivals. **Meinardus and Schleicher** describe the implementation of 3-D time-variant dip-moveout in the *f-k* domain. This method produces an impulse response with triplications and a real saddle shape as predicted by theoretical studies. **Ata et al.** use multicomponent seismic data to estimate near-surface elastic parameters at a test site in east Texas. Effects of anisotropy and heterogeneity are better identified with a combination of full wavefield surface and buried receiver observations. **Lazear** notes that while the second-order covariance function (autocorrelation) of seismic data has no phase, higher-order covariance functions (cumulants) retain the phase of the wavelet. He uses the fourth-order cumulant to recover the shape of a mixed-phase wavelet when the reflectivity is non-Gaussian, stationary, and statistically independent. **Kennett** uses a two-layer stacking procedure to provide a more accurate representation of the time behavior of reflections than a simple moveout analysis. This procedure is particularly useful for reflections with a conversion to shear at a hard seafloor for which the largest amplitudes occur at long offsets, and it allows extraction of shear-wave interval velocities below the seabed.

Short note

Mackie and Madden investigate conjugate-direction relaxation solutions for the 3-D magnetotelluric modeling problem. They obtain good results when a partial inverse preconditioner is used in conjunction with a multiple scaling technique.

GEOPHYSICS, VOL. 58, NO. 7 (JULY 1993); P. 924–934, 9 FIGS.

Orthogonality in CSAMT and MT measurements

David E. Boerner*, Ron D. Kurtz*, and Alan G. Jones*

ABSTRACT

The electric and magnetic fields from a single plane-wave source on a one dimensional (1-D) earth, or a plane-wave source polarized parallel or perpendicular to strike on a two-dimensional (2-D) earth, are orthogonal. On a layered earth and in the far-field of a controlled source, the electric and magnetic fields are also orthogonal. Therefore, orthogonality of **E** and **H** data is a necessary condition to justify the application of 1-D or 2-D modeling algorithms having a plane wave source. A strict criterion to prove orthogonality, and thus provide a rationale for the choice of interpretation methods, can be defined directly in terms of field data. However, field data acquired in the intermediate and near-field of any electromagnetic (EM) source are generally not orthogonal, even on a plane-layered earth. Representing these nonorthogonal data in an orthogonal coordinate system can be misleading, particularly for the minor axis components of the polarization ellipses. Nonorthogonality also arises because of 3-D scattering, with one common example being the electric field response of near surface structure. An example of field data illustrates the nonorthogonality in CSAMT measurements caused by the response of surficial geology. In these EM data, the angle between **E** and **H** is a sensitive indicator of geological contacts and faults. Quantitative analysis of these data can be performed with the assumptions of a "bulk" 1-D earth (i.e., orthogonal **E** and **H** in the far-field) and purely galvanic scattering of the EM fields.

INTRODUCTION

Controlled-source audio-frequency magnetotellurics (CSAMT) is an electromagnetic (EM) exploration method based upon the natural source magnetotelluric (MT) method, but with one important difference, the source. MT sources are usually lightning discharges or current distributions in the upper atmosphere and ionosphere. The fields of these natural current sources are considered to be plane waves at the earth's surface. In comparison with spatially varying source fields, the numerical modeling of conductivity structures excited by plane-wave sources is relatively simple.

CSAMT methods rely on artificial (or controlled) sources to generate the desired EM fields. Man-made sources overcome the unpredictable nature of the atmospheric sources, thereby making the MT methodology available for production surveying. The analogy with MT methods exists because in the far-field of *any* EM source distribution on a layered earth the electric and magnetic fields obey the impedance relation derived by Tikhonov (1950) and Cagniard (1953). However, the exact location of the "far-field" is only strictly defined for a layered earth and is dependent upon the (unknown) conductivity structure of the earth, the frequency of the source field, the source characteristics, and the source/receiver separation.

While it is desirable to record CSAMT data in the far-field of a controlled source, there are practical limits imposed by the geometric decay of the EM fields and the requirement for large lateral separations. The source-receiver separation necessary for far-field conditions may become impossibly large if the frequency is decreased, particularly in crystalline environments. One of the most important aspects of CSAMT survey design and interpretation is defining the frequency range of the far-field of experimental data in order to use MT interpretation routines. This concern represents the essence of a discussion by Maurer (1988) and Szarka (1988) on a paper by Bartel and Jacobson (1987) regarding the interpretation of CSAMT data with two-dimensional (2-D) MT models. However, with the exception of excluding the near-field response, these discussions offer no quantitative method for determining the applicability of 1-D or 2-D MT interpretation methods, which are often employed without a priori justification.

This paper describes some aspects of the EM fields from a grounded bipole source in the framework of the orthogonality of the electric and magnetic fields. The intention is to illustrate the importance of orthogonality in EM data and to define a criterion for deciding if EM field data are indeed

Manuscript received by the Editor September 3, 1991; revised manuscript received September 17, 1992.
*Geological Survey of Canada, 1 Observatory Crescent, Ottawa, Ontario, Canada K1A 0Y3.

orthogonal. If data are orthogonal, the choice of subsequent modeling and inversion can be justified solely by data characteristics.

The controlled source example is also important in that it can be generalized to demonstrate the general characteristics of 3-D scattering via the equivalent source method (e.g., Morse and Feshbach, 1953, Chap. 7). With an understanding of the cause of nonorthogonality, it becomes possible to develop methods for interpreting nonorthogonal field data. Nonorthogonality is generally a physical characteristic of the source fields or arises because of 3-D scattering. While the fields of an arbitrary source are easily calculated for layered earth models and can be used to interpret one aspect of nonorthogonal field data, understanding the 3-D scattering response presents many problems. However, a restricted model of 3-D scattering that assumes the response of near-surface, small-scale structure is mostly frequency independent and dominant in the electric field. For this particular case, a simple method of analyzing the response of the surficial geology can be developed from orthogonality considerations.

ORTHOGONALITY IN EM DATA

The physical basis for the MT impedance relationships introduced by Tikhonov (1950) and Cagniard (1953) and modified by Neves (1957) is simple. A plane-wave source over a 1-D (layered) earth or, a plane-wave source polarized parallel or perpendicular to the strike of a 2-D earth, generate orthogonal electric and magnetic fields. For any other situation, the resultant electric **E** and magnetic **H** field vectors are only orthogonal in the far-field of the source on a 1-D earth, or along common lines of symmetry about both the source and the geological structure. Nonorthogonality of **E** and **H** could imply that the earth (or source) structure is 3-D or that the source is not polarized along or perpendicular to strike (resulting in a "mixing" of the fields from two polarizations).

As a direct indication of the "dimensionality" of the geological structure (or source), orthogonality of EM fields is obviously important in data interpretation. Orthogonality of **E** and horizontal **H** in any data set (e.g., MT or CSAMT) is a necessary, but not sufficient condition to justify 1-D or 2-D plane-wave modeling or inversion procedures. The dot product rule can easily be used to test for orthogonality in field data,

$$E_x H_x + E_y H_y = |E||H| \cos \phi. \tag{1}$$

Parameter ϕ is the angle between the two vectors, and it is assumed that the product $E_z H_z$ is negligible with respect to the product of the horizontal electric and magnetic field components.

There are a number of ways to confirm the hypothesis that the electric and magnetic fields are orthogonal. One method would be to assume $\cos \phi = 0$ and then examine the statistical relevance of the equation,

$$E_x H_x = -E_y H_y.$$

This approach requires a knowledge of the mean values of E_x, H_x, E_y, H_y and their respective variances. A student's t test (for an approximately normal distribution) or some variant on the Mann-Whitney test (a rank sum test) can then be used to confirm or deny the hypothesis of equality. While measurement precision can be represented in the statistical analysis, it does not take into account the misalignment of sensors. A preferred method would be to compute the apparent angle between **E** and **H** with an associated variance and compare this with 90 degrees $\pm \varepsilon$, where ε is the sensor alignment uncertainty. If $\phi \pm \Delta\phi$ differs from 90 degrees $\pm \varepsilon$ in a statistical sense, the fields must be considered nonorthogonal. As the mapping from fields to ϕ is nonlinear, the variance and mean of ϕ are best determined from Monte Carlo realizations of the field data. That is, a synthetic population of data, possessing a normal probability distribution, are generated from the mean and variance of the measured data. From this population of electric and magnetic field data, several estimates of ϕ are realized and a mean and standard deviation can be computed.

1-D CONTROLLED SOURCE DATA

Consider the fields of an infinitesimally small horizontal electric dipole (HED). Quasi-static conditions are assumed and the HED is situated on a uniform conducting half-space (e.g., Bannister, 1966; Wait, 1982). The fields at any point on the surface of the half-space are most easily expressed in cylindrical coordinates,

$$\begin{aligned} E_r &= \frac{I\,d\ell}{2\pi\sigma\xi^3} \cos(\theta - \theta')[e_r], \\ E_\theta &= \frac{I\,d\ell}{2\pi\sigma\xi^3} \sin(\theta - \theta')[e_\theta], \\ H_r &= \frac{I\,d\ell}{2\pi\xi^2} \sin(\theta - \theta')[h_r], \\ H_\theta &= \frac{I\,d\ell}{2\pi\xi^2} \cos(\theta - \theta')[h_\theta], \end{aligned} \tag{2}$$

where

$$\begin{aligned} e_r &= 1 + (1 + \gamma\xi)e^{-\gamma\xi}, \\ e_\theta &= 2 - (1 + \gamma\xi)e^{-\gamma\xi}, \\ h_r &= 3I_1K_1 - \frac{\gamma\xi}{2}(I_0K_1 - I_1K_0), \\ h_\theta &= -I_1K_1, \end{aligned} \tag{3}$$

and where the horizontal separation between the receiver $(r, \theta, z = 0)$ and the source point $(r', \theta', z = 0)$ is given by the law of cosines

$$\xi = \sqrt{r^2 + r'^2 - 2rr' \cos(\theta - \theta')}. \tag{4}$$

In these expressions I_n and K_n are the modified Bessel functions of the first and second kind, respectively. The arguments of the modified Bessel functions have been omitted but are always $(\gamma\xi/2)$ where $\gamma = \sqrt{i\omega\mu\sigma}$ is the EM propagation constant. The conductivity of the half-space is σ and the permeability of free space is μ. The product of current and dipole length Idl is the dipole moment. A

uniform half-space is the simplest of all earth models that still represents the general characteristics of grounded dipole excitation of a layered earth. This representation also contains the essential elements of layered earth excitation by a finite length electric bipole, although there are important differences in the near-field. Since the fields of any EM source on any layered earth must show translational and rotational invariance, there is no loss of generality in letting $r' = 0$ so the fields become a function only of r and θ.

To simplify these expressions, consider two important limiting cases. The high frequency (or far-field) limit can be evaluated by letting $|\gamma r|$ approach infinity. The modified Bessel functions for large arguments are adequately approximated by the first two terms in the series expansion giving

$$I_1 K_1 \to \frac{1}{\gamma r},$$

$$\gamma r(I_1 K_0 - I_0 K_1) \to \frac{2}{\gamma r}.$$

Thus,

$$e_r = 1,\ e_\theta = 2,\ h_r = \frac{2}{\gamma r},\ h_\theta = -\frac{1}{\gamma r}. \tag{5}$$

Using equations (1), (2), and (5) it can be seen that the electric and magnetic fields are orthogonal, and the resulting Cagniard-Tikhonov impedance definition derived from these components is exactly that of a plane wave source over a uniform half-space. This representation of the fields emphasizes that there is no source dependence in the transfer relationship between orthogonal components of the electric and magnetic field. However, the r^{-3} attenuation factor, coupled with a high-frequency response in the horizontal magnetic field components proportional to $\omega^{-1/2}$, makes it difficult to acquire data with a large signal-to-noise ratio in the far-field ($|\gamma r| \gg 1$) of the source.

The low-frequency (or near-field) limit is obtained by letting $|\gamma r| \to 0$,

$$I_1 K_1 \to \frac{1}{2},$$

$$\gamma r(I_1 K_0 - I_0 K_1) \to -2.$$

The fields in this limit are found from

$$e_r = 2,\ e_\theta = 1,\ h_r = \frac{1}{2},\ h_\theta = -\frac{1}{2}. \tag{6}$$

Clearly, the electric and magnetic fields in the near-field of a grounded dipole source on a uniform half-space are not orthogonal [from equations (1), (2), and (6)]. It is trivial to extend this result to include the case of an arbitrary-shaped bipole on any layered earth. The essential characteristic of this analysis is that the magnetic field azimuth and amplitude are only dependent upon the source/receiver geometry and source moment while the electric field is also a function of the 1-D conductivity structure. As the dc magnetic field azimuth is independent of $\sigma(z)$ (e.g., Edwards et al., 1978), orthogonal components of **E** and **H** do not define a useful impedance.

The two limits discussed above are quite restrictive ($|\gamma r| \gg 1$ and $|\gamma r| \ll 1$), and CSAMT data in crystalline environments may be more representative of the transition zone than either limit. A more interesting, and practical, aspect of the half-space model is to study the orthogonality of the field in the transition zone between the near- and far-field. Boerner and West (1989) show that data acquired in the intermediate zone are generally more sensitive to layered-earth structure than data in either the near- or far-field.

Figure 1 shows the EM response of a uniform half-space model discussed by Goldstein and Strangway (1975) and Sandberg and Hohmann (1982). The figure is a map view of apparent resistivity data from measurements made in one quadrant around a 500 m linear grounded bipole source for an excitation frequency of $f = 32$ Hz. The fields are sampled on a 50-m grid and the source is centered at the origin and is oriented along the x-axis. Only one quadrant is shown because of the symmetry exhibited about the source. The value plotted is the logarithm (base 10) of the apparent resistivity calculated from the Cagniard-Tikhonov relationship using the electric field parallel to, and magnetic field perpendicular to, the source axis (i.e., $\rho_a = |E_x/H_y|^2/\omega\mu$). The half-space resistivity is $\rho = 100\ \Omega \cdot$ m. A reasonable definition of the far-field is given by the region where the apparent resistivity is equal to the half-space resistivity and does not change appreciably with lateral distance. At large distances from the bipole, the apparent resistivity generally approaches the half-space resistivity, but there is substantial topography close to the source. The near-field artifact is well known and occurs because the fields are approximately static at low frequency, but the apparent resistivity is inversely proportional to frequency. Of more importance than the near-field is the region of anomalous apparent resistivity extending from the bipole source to very large radial distances. Along this line, the major axis of the electric field polarization ellipse is predominantly in the y-direction meaning that the apparent resistivity is defined using the minor axes components.

Figure 2 shows the angle between the major axes of the electric and magnetic field polarization ellipses (e.g., Born and Wolf, 1965) on the same grid as Figure 1. The angle between the major axes tends to oscillate with distance from the source and undergoes a step discontinuity along a line extending from the bipole grounding point. From Figures 1 and 2, it is clear that artifacts appear in the apparent resistivity when the minor components of nonorthogonal polarization ellipses are used to define apparent resistivity. The amplitude of the ridge in Figure 1 is essentially unrelated to the half-space resistivity and would tend to infinity if the magnetic field were linearly polarized. Similarly, if the electric field were linearly polarized, the points at which E_x disappears would result in a zero apparent resistivity. However, in the transition zone between near-field and far-field the EM fields are generally elliptically polarized. Thus, there is always a minor axis of the polarization ellipse and the apparent resistivity remains finite but greater than zero (unlike the case in the near- and far-field limits).

This numerical example illustrates a case of nonorthogonal behavior in EM fields and some ramifications of analyzing orthogonal component data, particularly when the field components are more strongly dependent upon geometry

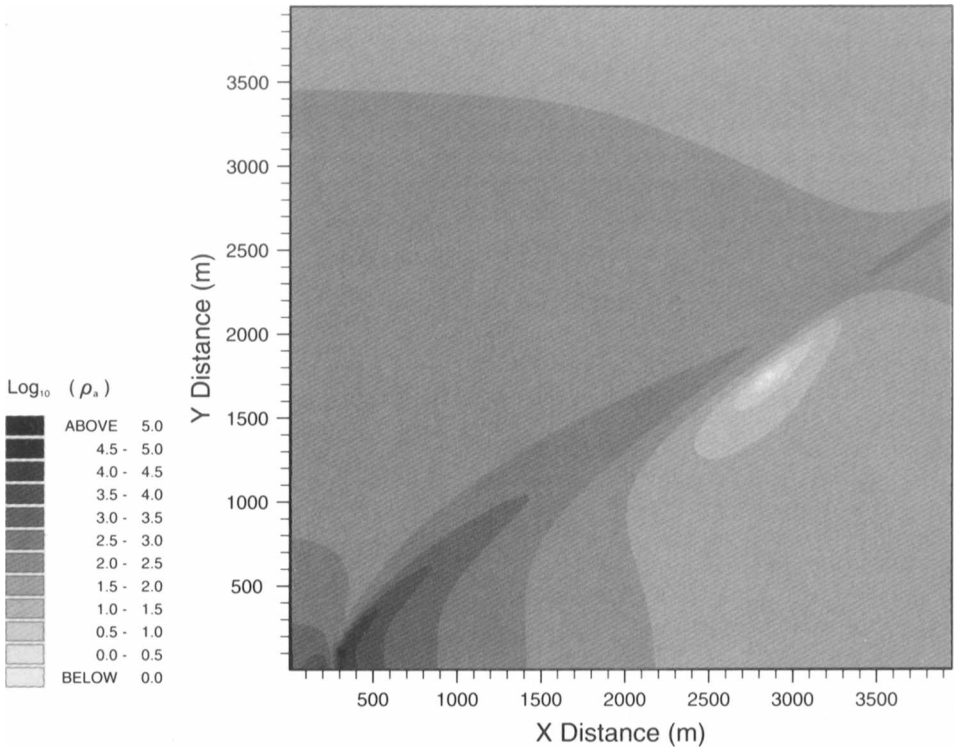

FIG. 1. A contour map of the logarithm (base 10) of the Cagniard-Tikhonov apparent resistivity calculated in one quadrant around a linear grounded bipole on a uniform half-space ($\rho = 100\ \Omega \cdot m$). The bipole extends 500 m along the x-axis and is centered at $x = 0$. Apparent resistivity is calculated from E_x and H_y.

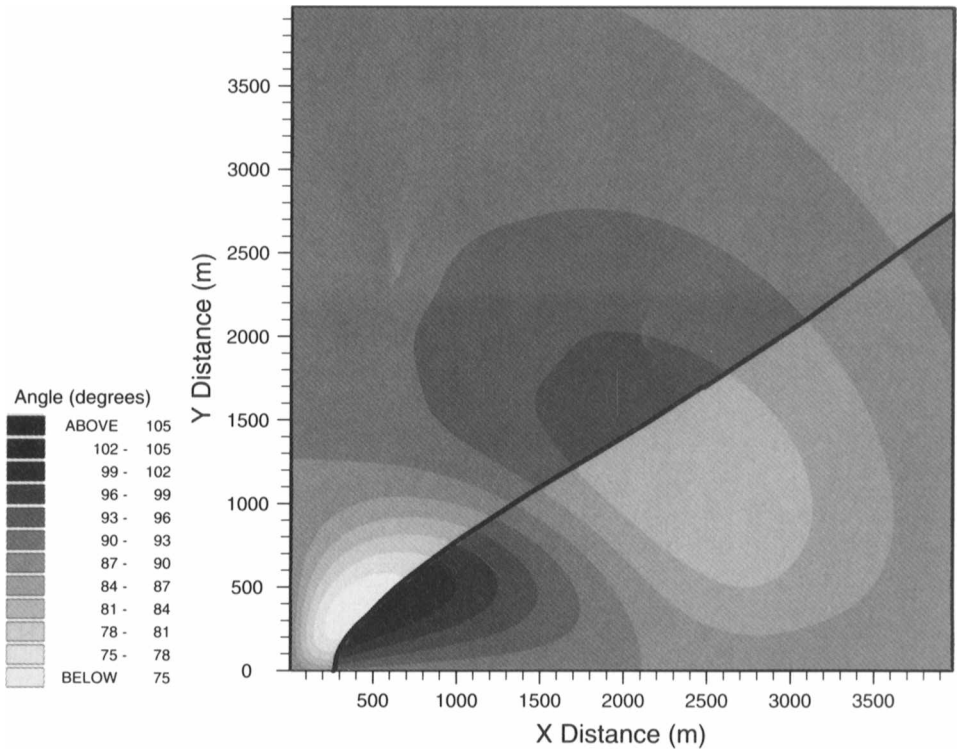

FIG. 2. A contour plot of the angle between the major axes of the horizontal electric and magnetic field polarization ellipses around a grounded bipole on a uniform half-space described in Figure 1. Darker shading indicates angles greater than 90 degrees. Compare the location of the discontinuity in the angle surface with the apparent resistivity artifacts plotted in Figure 1. Note the oscillatory nature of the angle between the electric and magnetic fields as a function of distance from the bipole.

than conductivity. When the earth is quasi-layered, measurement locations can be restricted to regions where the fields have little curvature, thus avoiding the problems of nonorthogonal data. A less restrictive, yet robust, alternative is a definition of apparent resistivity calculated from the lengths of the major axes of the ellipses of polarization without regard for the angle between the axes. The Cagniard-Tikhonov apparent resistivity calculated using this definition is shown in Figure 3 and contains only the near-field artifact. The nonlinear equations in (2) and (3) are easily inverted numerically for apparent resistivity and the near-field artifacts in Figure 3 can be eliminated.

Figure 3 is a trivial example but it illustrates how a definition of apparent resistivity using ellipse major axes data is natural for the near-field, transition zone, and far-field of a grounded source on a uniform half-space. The principal justification for this definition is that the magnitude, and not the azimuth, of the magnetic field vector is used for defining an EM transfer relationship. As stated earlier, the azimuth of the magnetic field is purely dependent upon source/receiver geometry for a 1-D earth in the near-field. Thus, the major axes apparent resistivity will also be appropriate for an arbitrary layered earth and, in the near-field, acts as a true normalization of the electric field for the EM source moment. However, the use of nonorthogonal data for apparent resistivity calculations would be most useful if accompanied by the angle between **E** and **H** which may be indicative of geological structure.

GALVANIC SCATTERING OF ELECTRIC FIELDS

The discussion to this point has dealt with the response of only a layered earth to electric bipole excitation. Such examples are not only relevant in terms of idealized experiments and simplified interpretations, but are also representative of 3-D EM scattering because of the duality between sources and boundary conditions. Duality permits any scattering body to be replaced by an "equivalent source" distribution, subject to the constraint that the fields of the equivalent sources match the boundary conditions imposed by the conductivity structure of the scattering body. This means that the scattering currents from some local heterogeneity can be represented by electric dipole sources, and the horizontal dipole source examples from the previous sections become relevant for understanding 3-D scattering currents. In the context of this discussion, the fields from the equivalent sources are generally nonorthogonal unless the observation site is in the far-field of the entire current distribution (including the artificial source and all equivalent sources that represent geological structures). It is not sufficient to consider what defines the far-field of each source distribution individually since the superposition of orthogonal fields is not necessarily orthogonal. This can be seen algebraically by writing the dot product rule for orthogonal vectors and assuming there are n scattering bodies (superscript s) excited by the primary (superscript P) fields since

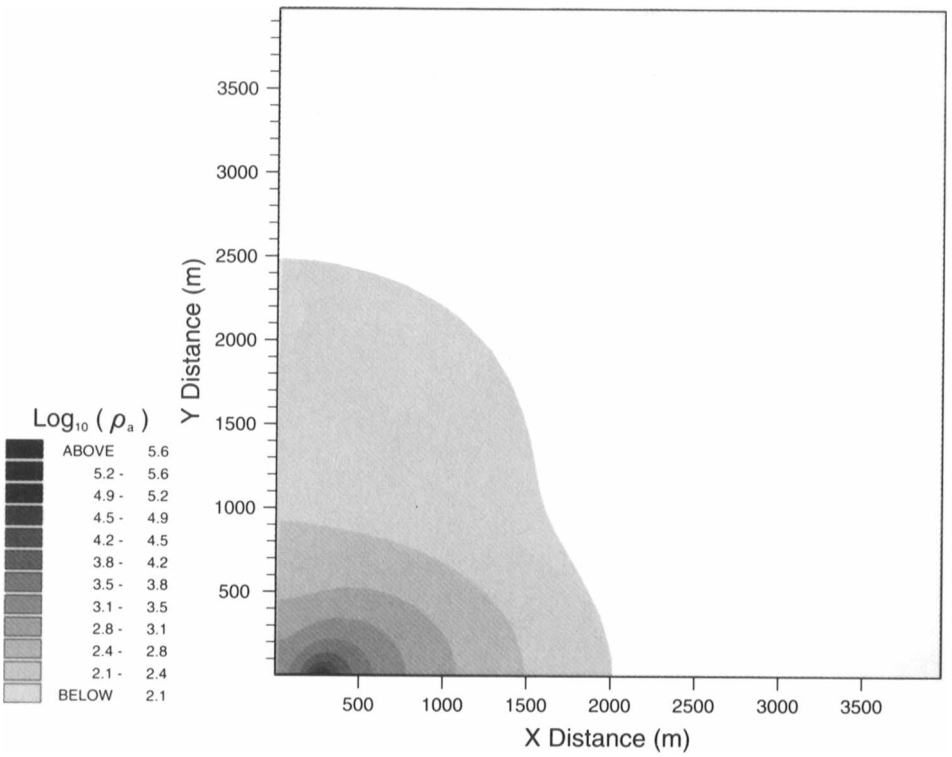

FIG. 3. A contour map of the apparent resistivity calculated for the model described in Figure 1. The surface represents the logarithm (base 10) of the Cagniard-Tikhonov apparent resistivity calculated from the major axes magnitudes of the electric and magnetic field polarization ellipses. The resistivities are greater than or equal to 100 Ω · m.

$$\left(E_x^P + \sum_i^n E_{x,i}^s\right)\left(H_x^P + \sum_i^n H_{x,i}^s\right)$$

$$\neq -\left(E_y^P + \sum_i^n E_{y,i}^s\right)\left(H_y^P + \sum_i^n H_{y,i}^s\right)$$

even if $E_x^P H_x^P = -E_y^P H_y^P$ and $E_{x,i}^s H_{x,i}^s = -E_{y,i}^s H_{y,i}^s$, for all i. Orthogonality can only be assured in the extremely restrictive and unrealistic scenario that the entire source distribution is localized near the transmitter. If there is any nonlayered geological structure (equivalent sources) near the receiver, the total EM fields are generally nonorthogonal.

An important subset of the equivalent source scattering model is to consider a measurement site in the near-field of the scattering current distribution. By virtue of the almost frequency independent nature of the near-field response, this scenario is sometimes called galvanic scattering (e.g., Bahr, 1991, Groom and Bailey, 1991, Torres-Verdín and Bostick, 1992). Galvanic scattering occurs dominantly as the result of charge accumulation on conductivity gradients and is a very important concern, particularly for crystalline terrains. This response is seen primarily in the electric field and, to a lesser extent, in the magnetic field. Galvanic scattering represents important geoelectric information, and it is possible to quantify the amount and spatial characteristics of galvanic scattering in the measured electric fields through the use of orthogonality arguments.

We begin by assuming that the response of surficial, local, small scale structure is a galvanic (frequency independent) distortion of the electric fields, but that the magnetic fields are unaffected. Also, the underlying (bulk) earth is assumed to be 1-D. At any site around the source, and within these assumptions, the measured electric field (E_x^M, E_y^M) is the sum of the 1-D electric field plus the contribution of the scattered currents. That is,

$$\begin{bmatrix} E_x^M \\ E_y^M \end{bmatrix} = \begin{bmatrix} \cos\psi & -\sin\psi \\ \sin\psi & \cos\psi \end{bmatrix} \begin{bmatrix} 1 + C_\parallel \\ C_\perp \end{bmatrix} E_{1-D},$$

where E_{1-D} is the magnitude of the undisturbed (1-D) electric field vector. Parameter ψ is the angle between E_{1-D} and the x-measurement direction, and the rotation matrix simply maps between the undisturbed electric field direction

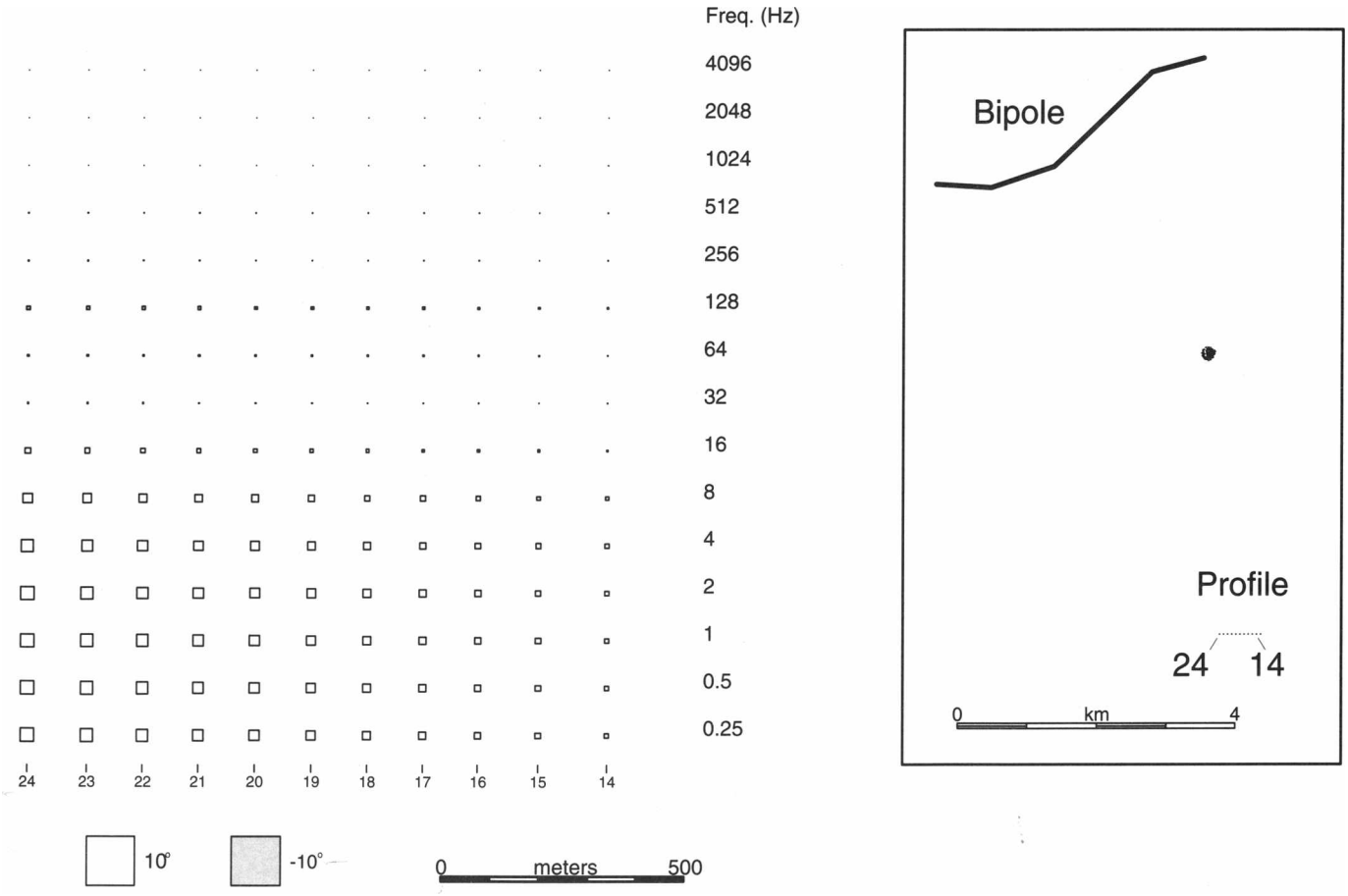

FIG. 4. The angle between the major axes of the electric and magnetic field polarization ellipses as a function of lateral position and frequency computed for a grounded bipole on a layered earth. The length of a side on each square is proportional to the deviation from 90 degrees. Angles less than 90 degrees are shaded. The inset illustrates the source/receiver geometry and scale. In the far-field of the source the horizontal field components are orthogonal and the squares collapse into dots. The geometry and station numbering is consistent with that of the field example in Figures 7 through 9.

and the measurement direction. The direction of E_{1-D} is defined here as the azimuth of the major axis of polarization, although in the far-field E_{1-D} is linearly polarized, and there is no confusion about the meaning of the $\|$ direction.

$C_\|$ and $C_\perp$ are real, frequency-independent constants related to the dipole moment and position of equivalent sources that represent the galvanic response of the scattering body. This can be seen by simply considering the HED contribution to the equivalent source distribution and treating equations (2) and (6) as the scattered fields from a current source proportional to E_{1-D}. The exact values of $C_\|$ and $C_\perp$ can only be calculated by finding the equivalent source distribution and integrating over the source volume. $C_\|$ is the fraction of E_{1-D} scattered in the $\|$ direction, while $C_\perp$ is the field scattered in the perpendicular direction. When this equation is rewritten as

$$\begin{bmatrix} \cos\psi & \sin\psi \\ -\sin\psi & \cos\psi \end{bmatrix} \begin{bmatrix} E_x^M \\ E_y^M \end{bmatrix} = \begin{bmatrix} 1 + C_\| \\ C_\perp \end{bmatrix} E_{1-D},$$

it is clear that by applying the inverse rotation from the measurement axis to the direction of the "1-D" electric field, an estimate of the galvanic scattering can be obtained from

$$\frac{E_y^M \cos\psi - E_x^M \sin\psi}{E_y^M \sin\psi + E_x^M \cos\psi} = \frac{C_\perp}{1 + C_\|}. \tag{7}$$

The difficulty with this representation is that the azimuth of the undisturbed (1-D) electric field is generally unknown. However, if the data were acquired in the far-field of the source, the 1-D electric field would be orthogonal to the 1-D magnetic field (which is assumed to be undisturbed by the local, near-surface structure). The angle ψ is thus 90 degrees from the magnetic field (major axis) polarization direction. If the ratio $C_\perp/(1 + C_\|)$ is a real constant (zero imaginary component) over some bandwidth at high frequency, the data are consistent with the assumption of galvanic scattering in the far-field of the source. This frequency-independent

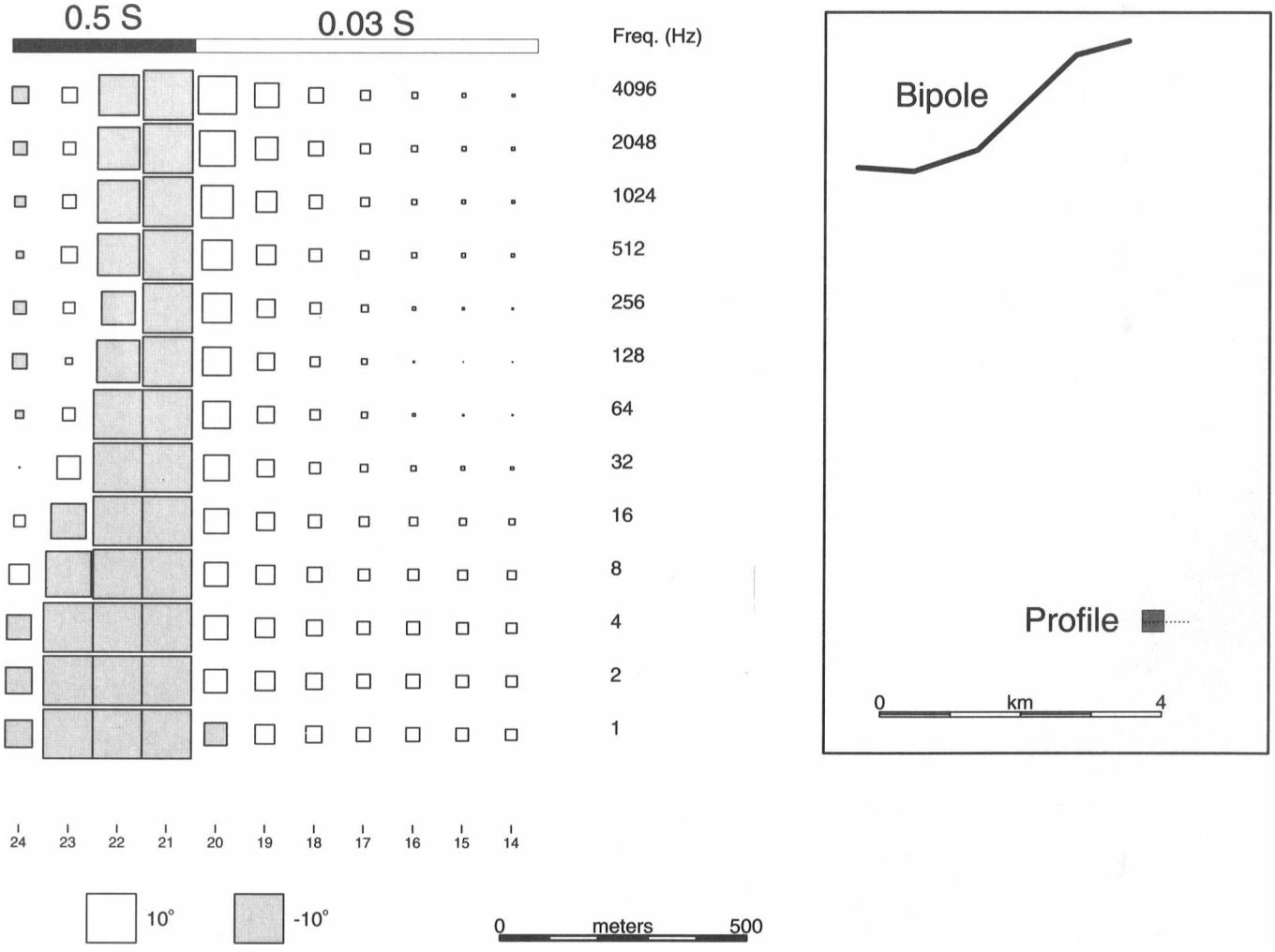

FIG. 5. Orthogonality data computed for the same layered earth model used to calculate the data in Figure 4 with the addition of an conductive thin sheet on the surface of the earth beneath the measurement sites (inset). The anomalous region is a 400 × 400 m square having conductance of 0.5 S.

behavior is equivalent to the condition that the electric field azimuth should not change as a function of frequency in the case of galvanic scattering. The important caveat is that this analysis is only meaningful under the above assumptions, and, in particular, the high-frequency magnetic fields must show evidence of 1-D behavior.

The application of the orthogonality analysis can be demonstrated with some examples. Figure 4 shows the angle between the major axes of the polarization ellipses for electric and magnetic fields calculated on a 1-D earth. The earth model consists of a 2000-Ω · m layer 1500-m thick, over a 6000-Ω · m half-space. The profile line is one kilometer in length and approximately 7.5 km from a 4 km long bipole. This geometry will be used for the remaining examples. The data are presented as a function of frequency (ordinate) and location along the profile line (abscissa). The length of a side of the squares is determined by subtracting 90 degrees from the angle between the major axes of the electric and magnetic field polarization ellipses. As expected from Figure 4, there is an oscillatory transition between the near- and far-field with the near-field being strongly nonorthogonal. In the transition zone between 128 and 4 Hz, the angle between **E** and **H** oscillates between greater than 90 degrees and less than 90 degrees. For this particular source/receiver configuration, the near-field (low frequency) electric and magnetic fields are all greater than 90 degrees apart.

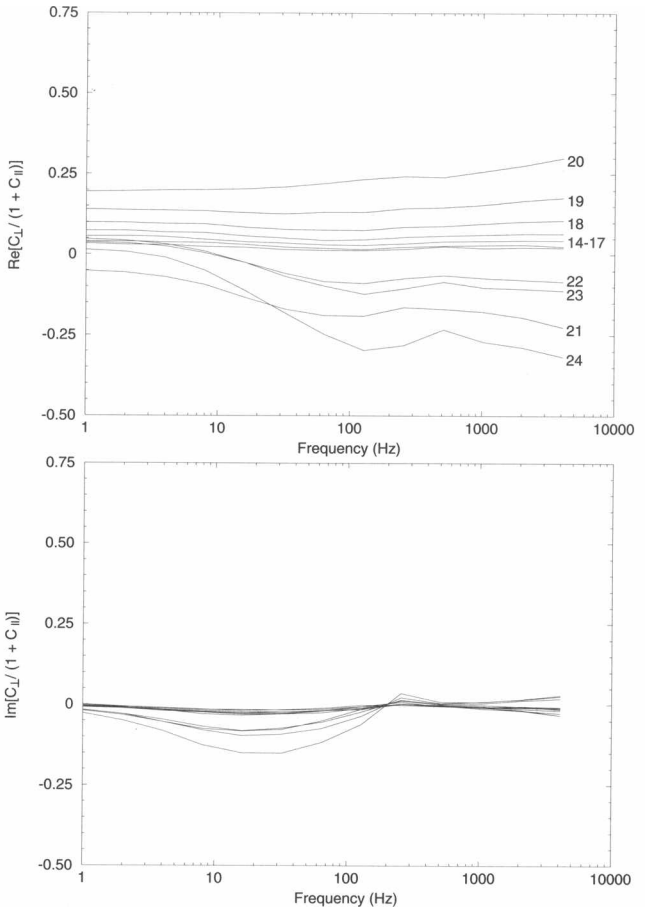

FIG. 6. Galvanic distortion analysis of the data shown in Figure 5. The sites off the structure show little variation throughout the entire frequency band, while those on the inhomogeneous conductance distribution illustrate the changing proportion of fields scattered in the ⊥ direction (defined relative to the magnetic field azimuth). Note that the amplitude of the distortion decreases with distance from the edge of the sheet.

Figure 5 shows the response of a 3-D body that is confined to a thin sheet (Vasseur and Weidelt, 1977) at the surface of the layered earth model used in Figure 4. The anomalous thin sheet was a square plate, 400 × 400 m and is illustrated in Figure 5. The source/receiver configuration is unchanged from Figure 4 permitting direct comparisons of the far-field frequency range. There is significant electric field scattering from the thin sheet, and at the frequencies that were considered far-field on the layered earth, the electric and magnetic fields are not orthogonal.

Galvanic scattering [equation (7)] was estimated for the thin sheet modeling results and the result is shown in Figure 6 as plots of the real and imaginary parts of the ratio $C_\perp/(1 + C_\parallel)$. Stations 14–20 produce a relatively constant ratio that is almost entirely real. The amplitude of the ratio (essentially a measure of the field scattered in the ⊥ direction) decreases with distance from the scattering body. However, the ratios for stations 21–24 vary as a function of frequency and are only real at low frequencies and above 100 Hz. These data illustrate the magnitude of the electric field scattering evident in Figure 5 by the nonorthogonality of the electric and magnetic fields. The analysis shown in Figure 6 indicates that the data are consistent with the galvanic scattering hypothesis and suggest that interpretation could be based on a layered earth model. Note, however, that it would be inappropriate to invert the orthogonal components of the measured field because of the strong scattering in the ⊥ direction (≈25 percent of E_{1-D} for site 24). Also, E_{1-D} can only be determined to within a multiplicative constant from single site data since only the ratio of the scattering constants $C_\parallel$ and $C_\perp$ can be found.

The analysis applied assumes that the electric and magnetic fields are orthogonal, which is not true in the near-field. Thus, while it is tempting to interpret the low-frequency behavior exhibited in Figure 6 in terms of the geologic structure, the estimates of the scattering in the parallel and perpendicular directions are not quantitative in the near-field. However, over small distances the 1-D magnetic and electric field do not vary substantially, and qualitative information regarding the low-frequency scattering can be obtained from multiple station data.

Figure 7 is similar to Figures 4 and 5, but shows the orthogonality plots from CSAMT field data collected in the central volcanic belt near the Buchans Mine, Newfoundland (Boerner et al., 1990; Boerner et al., 1992). The Buchans group consists predominantly of a bimodal suite of basalt and rhyolite that is thought to have formed during a period of tectonic extension following calc-alkaline constructive arc volcanism (Thurlow and Swanson, 1987). The structural setting of Buchans is that of a fold and thrust belt, making structural mapping a critical component in understanding the nature and setting of the ore horizons. The purpose of the CSAMT survey was to map geological features on the surface and at a depth to complement structural interpretation based primarily upon high-resolution seismic reflection

methods. The complete data set is large, and only a subset of the data that illustrate the nonorthogonality of **E** and **H** will be discussed here. The plots in Figure 7 clearly indicate that the EM fields are not orthogonal and vary rapidly over short distances. Consequently, the data are not representative of the far-field response from a 1-D structure. The magnetic field data do not vary substantially along the profile in the frequency band recorded, suggesting more lateral uniformity than is evident in the electric fields.

Figure 8 illustrates the results of the galvanic scattering study. There are some similarities with Figure 6, but generally the magnitude of the C ratio is much larger in the field data and may not be adequately represented by a simple thin sheet model. One correlation between the simple model and the data is that the real part exhibits strong frequency dependence for stations 20–24 (bold lines) and a relatively flat spectrum for the remaining stations.

The anomalous regions in Figures 7 and 8 correspond well with the mapped geological structure (Figure 9). The four stations on the western end of the profile (stations 21 to 24) are distinct from the rest of the line because $\angle$**EH** is less than 90 degrees (with the puzzling exception of site 19). These sites were located in the felsic volcaniclastics of the Lundberg Hill formation while the rest of the line crosses the mafic volcanics of the Ski Hill formation. The orthogonality of the field components and the galvanic analysis highlight the presence of geological contacts and faults in the CSAMT measurements. Detailed fitting of these data is better accomplished in terms of the EM fields, but is hampered by the severe limitations on the spatial sampling and restrictions on 3-D numerical modeling routines. Also, the apparent structure in the "pseudosection" of the angle plots in Figure 7 is not necessarily representative of conductivity variations at depth. Variations in the angle between **E** and **H** as a function of frequency is governed by the amplitude and direction of the scattered fields as well as the behavior of the "background" 1-D fields from the bipole source. Without measurements on a grid, interpretation of this data will be, at best, qualitative.

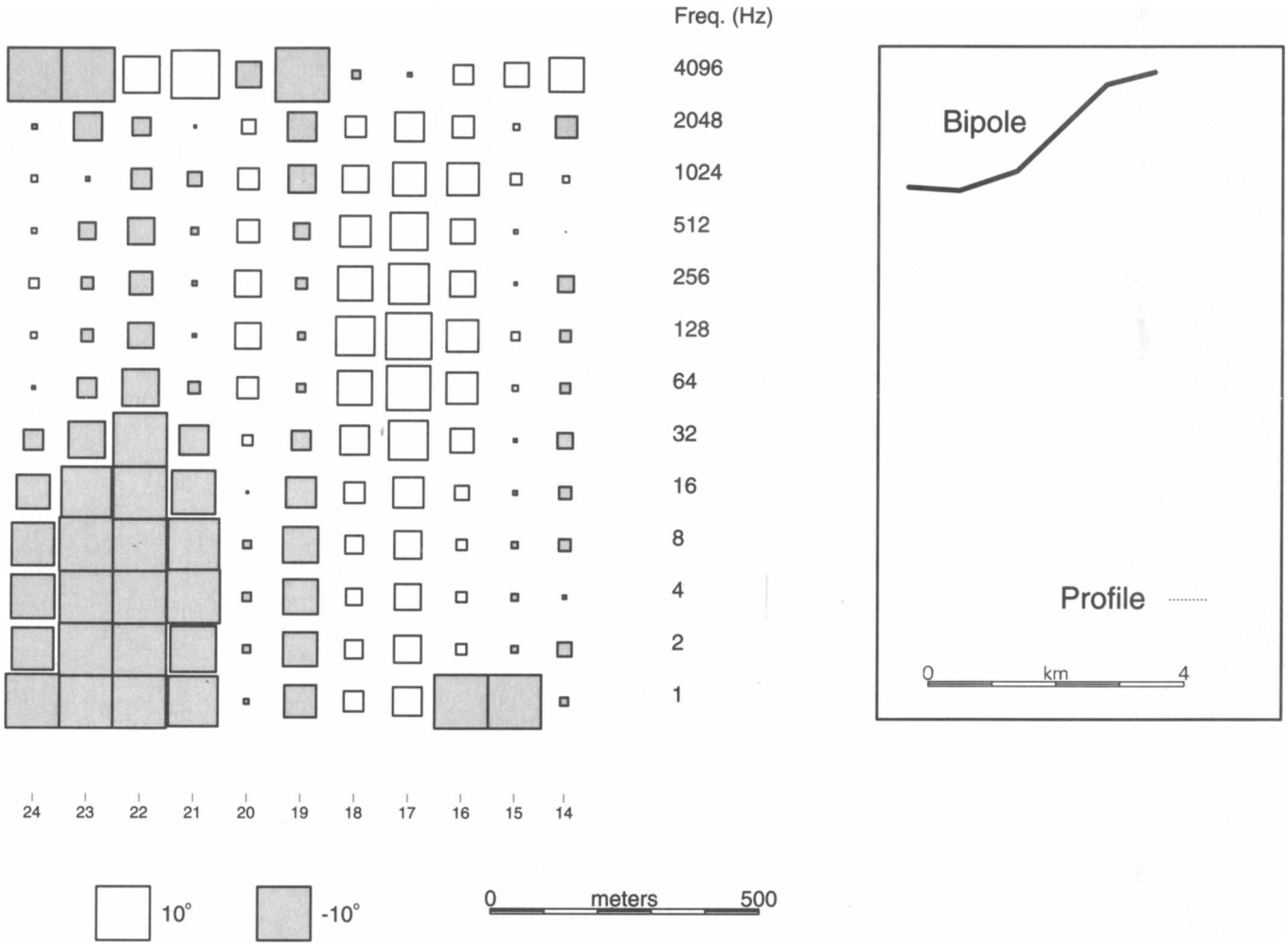

FIG. 7. Deviations from orthogonality calculated from actual field data collected near the Buchans mine in central Newfoundland. The "normal" earth model in the vicinity is similar to the layered model used in calculating Figure 5, but there are obvious 3-D effects in the field data that preclude modeling with MT plane-wave algorithms. Uncertainties are not illustrated in this figure, but below 1000 Hz, the variation in ϕ is usually less than 2 degrees. Sensors were aligned to within 1 degree.

DISCUSSION

Orthogonality of the electric and magnetic fields is a necessary but not sufficient condition for using plane-wave source models over 1-D and 2-D earths (assuming the sources are either parallel or perpendicular to strike). Nonorthogonality in field data implies that the earth is 3-D, that the source is not polarized parallel or perpendicular to strike, or that data were not acquired in the far-field of the source. The requirement for orthogonality has strong implications for the interpretation of CSAMT data and provides a means of justifying the use of plane-wave source numerical modeling algorithms. Although, in general, CSAMT surveys are best planned and interpreted with explicit consideration of the source characteristics.

Establishing the orthogonality of **E** and **H** requires at least "vector" (four components of the horizontal EM field components) measurements of the electric and magnetic field. "Scalar" (one set of orthogonal components of **E** and **H**) CSAMT measurements provide absolutely no independent information about whether plane-wave modeling of the source field is appropriate and could produce highly misleading results. Tensor CSAMT (e.g., Li and Pedersen, 1991) is an attractive means of dealing with some of the problems of data nonorthogonality on a layered earth, but at the price of nearly doubling data acquisition costs and imposing restrictions on the field logistics. Multiple sources are, without doubt, the optimal method of resolving 3-D structure, but are redundant on a purely layered earth.

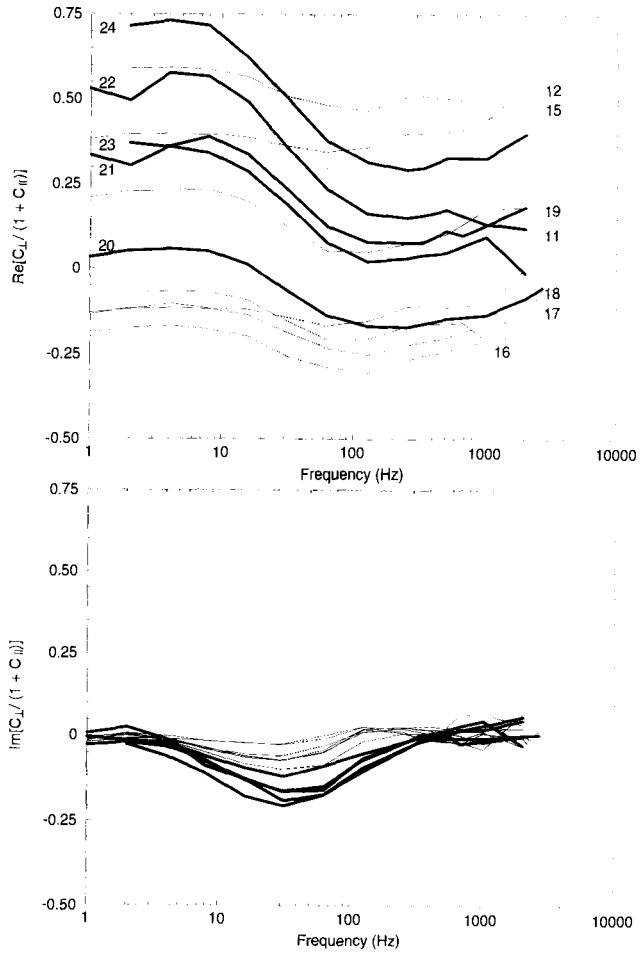

FIG. 8. Galvanic distortion analysis of the field data. Over the band from 100 to 2000 Hz the field data can be approximately represented by far-field galvanic scattering. Heavy lines indicate stations on the felsic volcanics and the numbers refer to the sites shown in Figure 9.

Misalignment of electric and magnetic sensors is an important factor to consider in assessing the orthogonality of field data. Field layout errors of a few degrees in orientation could result in the appearance of nonorthogonality, even when the EM fields are truly orthogonal. Furthermore, misalignment of a controlled source near a 2-D earth would generate nonorthogonal fields. In this regard, some care must be taken to ensure that the field experiment provides the appropriate data required for interpretation.

When the EM fields are judged to be nonorthogonal, the value of an impedance calculated from a ratio of orthogonal components of **E** and **H** becomes questionable. Of course, the actual definition of the impedance is irrelevant for modeling if a consistent system is used for both the data and the calculated model response *and* if the model is an adequate representation of the earth. For example, in the near-field **H** is nearly independent of $\sigma(z)$ and the magnitude of the magnetic field is essentially an estimate of source moment. The magnitude of the orthogonal components of **H** are, however, dependent on the source/receiver geometry and the source moment. With single source data, a robust apparent resistivity can be defined from the length of the polarization ellipse major axes. For multiple source data, such estimates could be derived from rotationally invariant measures of the impedance tensor (e.g., Li and Pedersen, 1991). However, these measures inevitably reduce the information content, and one very important result of this study is that the degree of nonorthogonality in EM data is a strong indicator of lateral structure.

It is possible to test for the presence of galvanic scattering in controlled-source EM data based on an assumed orthogonality of the electric and magnetic fields. This analysis has proved quite useful in appraising and understanding field data as it gives a direct (but fractional) estimate of the scattered electric fields. Moreover, the analysis lends some confidence to the interpretation of EM data in terms of simplified (e.g., 1-D) models.

ACKNOWLEDGMENTS

It is a pleasure to acknowledge stimulating discussions with Prof. L. B. Pedersen and his careful review of the manuscript. Jim Craven and Ross Groom are thanked for their enthusiastic, timely, and insightful reviews and discussions. Laurie Reed stimulated many aspects of the Buchans project, and his guidance and insight have proven very valuable. The data were acquired with joint funding from B. P. Canada Ltd. (Mining Division), Lithoprobe, and the GSC. This is Geological Survey of Canada publication number 27891. Lithoprobe publication number 440.

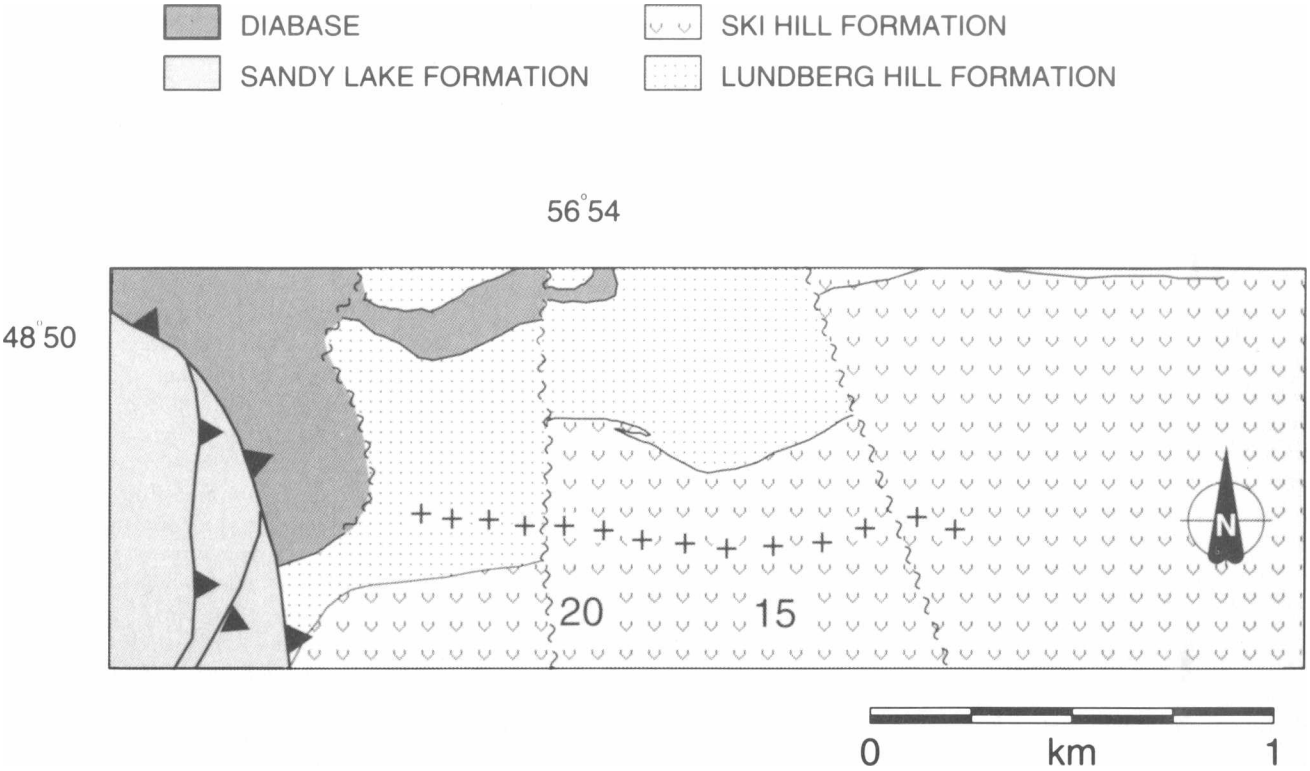

FIG. 9. Detailed geological map of the CSAMT receiver site locations to indicate the location of known or inferred contacts, faults, and thrust faults. The presence of the tear fault between stations 20 and 21 is clearly indicated in the nonorthogonality of the EM field data shown in Figures 7 and 8.

REFERENCES

Bannister, P. R., 1966, Quasi-static fields of dipole antennas at the earth's surface: Radio Sci., **11**, 1321–1330.

Bahr, K., 1991, Geological noise in magnetotelluric data: A classification of distortion types: Phys. Earth and Planet. Int., **66**, 24–38.

Bartel, L. C., and Jacobson, R. D., 1987, Results of a controlled-source audio-frequency magnetotelluric survey at the Puhimau thermal area, Kilauea Volcano, Hawaii: Geophysics, **52**, 665–677.

Boerner, D. E., and West, G. F., 1989, A spatial and spectral analysis of the electromagnetic sensitivity in a layered earth: Geophys. J., **98**, 11–21.

Boerner, D. E., Spencer, C. P., Wright, J. A., Carroll, P., and Reed, L. E., 1990, High-resolution seismic and EM at the Buchans Mine Newfoundland: Eng. and Min. J., **191**, 25–29.

Boerner, D. E., Wright, J. A., Thurlow, J. G., and Reed, L. E., 1992, Tensor CSAMT Studies at the Buchans Mine in central Newfoundland: Geophysics, **58**, 12–19.

Born, M., and Wolf, E., 1965, Principles of optics: Pergamon Press.

Cagniard, L., 1953, Basic theory of the magnetotelluric method of geophysical prospecting: Geophysics, **18**, 605–635.

Edwards, R. N., Lee, H., and Nabighian, M. N., 1978, On the theory of magnetometric resistivity (MMR) methods: Geophysics, **43**, 1176–1203.

Groom, R. W., and Bailey, R. C., 1991, Analytic investigations of the effects of near-surface three-dimensional galvanic scatterers on MT tensor decomposition: Geophysics, **56**, 496–518.

Goldstein, M. A., and Strangway, D. W., 1975, Audio-frequency magnetotellurics with a grounded electric dipole source: Geophysics, **40**, 669–683.

Li, X., and Pedersen, L. B., 1991, Controlled-source tensor magnetotellurics: Geophysics, **56**, 1456–1461.

Maurer, H.-M., 1988, Discussion on: "Results of a controlled-source audio-frequency magnetotelluric survey at the Puhiman thermal area, Kilauea Volcano, Hawaii", by L. C. Bartel, and R. D. Jacobson: Geophysics, **53**, 724–725.

Morse, P. M., and Feshbach, H., 1953, Methods of theoretical physics, Parts I and II: McGraw-Hill Book Co. Inc.

Neves, A. S., 1957, The magnetotelluric method in two-dimensional structures: Ph.D. thesis, Mass. Inst. Tech.

Sandberg, S. K., and Hohmann, G. W., 1982, Controlled-source audio magnetotellurics in geothermal exploration: Geophysics, **47**, 100–116.

Szarka, L., 1988, Discussion on: "Results of a controlled-source audio-frequency magnetotelluric survey at the Puhiman thermal area, Kilauea Volcano, Hawaii", by L. C. Bartel and R. D. Jacobson: Geophysics, **53**, 726–727.

Thurlow, J. G., and Swanson, E. A., 1987, Stratigraphy and structure of the Buchans Group: In Buchans Geology, Newfoundland, R. V. Kirkham, Ed., Geol. Sur. of Can., Paper 86-24, 35–46.

Tikhonov, A. N., 1950, Determination of the electrical characteristics of the deep strata of the earth's crust: Dok. Akad. Nauk. SSSR, **73**, 295–297.

Torres-Verdín, C., and Bostick, F. X., 1992, Implications of the Born approximation for the magnetotelluric problem in three-dimensional environments: Geophysics, **57**, 587–602.

Vasseur, G., and Weidelt, P., 1977, Bimodal electromagnetic induction in nonuniform thin sheets with an application to the northern Pyrenean induction anomaly: Geophys. J. Roy. Astr. Soc., **51**, 669–690.

Wait, J. R., 1982, Geoelectromagnetism: Academic Press, Inc.